ChemComm

ROYAL SOCIETY OF CHEMISTRY

COMMUNICATION

View Article Online
View Journal | View Issue

Check for updates

Cite this: *Chem. Commun.*, 2020, **56**, 11977

Received 20th June 2020,
Accepted 1st September 2020

DOI: 10.1039/d0cc04299d

rsc.li/chemcomm

Peptide nanotubes self-assembled from leucine-rich alpha helical surfactant-like peptides†

Valeria Castelletto,[a] Jani Seitsonen,[b] Janne Ruokolainen,[b] Cristian Piras,[a] Rainer Cramer,[a] Charlotte J. C. Edwards-Gayle[c] and Ian W. Hamley*[a]

The designed arginine-rich surfactant-like peptide R_3L_{12} (arginine$_3$–leucine$_{12}$) is shown to form a remarkable diversity of self-assembled nanostructures in aqueous solution, depending on pH, including nanotubes, mesh-like tubular networks in three-dimensions and square planar arrays in two-dimensions. These structures are built from α-helical antiparallel coiled–coil peptide dimers arranged perpendicular to the nanotube axis, in a "cross-α" nanotube structure. The aggregation behavior is rationalized based on the effects of dimensionality, and the balance of hydrophobic and electrostatic interactions. The nanotube and nanomesh structures display arginine at high density on their surfaces, which may be valuable for future applications.

Peptide nanotubes are biomolecular self-assemblies with remarkable structural and functional properties.[1–14] Several classes of peptide nanotube have been reported including those based on helically wrapped β-sheets,[15–20] laminates of cyclic peptide dimers forming antiparallel β-sheet stacks,[10,21,22] and stacks of alternating D,L-cyclic peptides stabilized by hydrogen bonded antiparallel β-sheets.[1,7,23] In addition, the parallel packing of coiled coil peptide arrays can lead to tubular structures.[24–26] Here, we report on a distinct class of peptide nanotube based on a designed surfactant-like peptide (SLP).[27] We have recently reported on the self-assembly of a number of SLPs with hydrophobic alanine repeats and various charged 'headgroups'. These form β-sheet nanofibrils,[28,29] and in some cases nanotubes.[19,20,30]

Here, we explore the self-assembly of SLPs containing leucine repeats instead of alanine sequences, since leucine has a strong α-helix propensity.[31] The peptide studied is R_3L_{12} (and is capped at both termini, ESI,† Scheme S1). In dilute aqueous solution, nanotube structures comprising α-helical peptide dimers stacked perpendicular to the walls were observed, which have a thickness that corresponds to the length of the dimer comprising antiparallel α-helical peptides. We also unexpectedly observed continuous nanotubular channel network structures that are accessible *via* pH variation. These structures present arginine residues at the surfaces of the nanotube and tubular network structures, providing a highly cationic surface for future applications. In addition, an ordered square lattice array was observed in thin films under certain conditions of pH. We rationalize the formation of this diverse range of previously unreported peptide nanostructures on the basis of the balance between hydrophobic and electrostatic effects.

We studied pH-dependent self-assembly of R_3L_{12} at pH 4 (native), or lower, pH values being tuned by addition of 10 mM HCl (pH 2) or 100 mM HCl (pH 1). Circular dichroism (CD) spectra shown in Fig. 1, measured for 0.04 wt% R_3L_{12}, confirm the formation of α-helical coiled coil structures for all solution conditions studied (the CD spectra for 0.07 wt% solutions

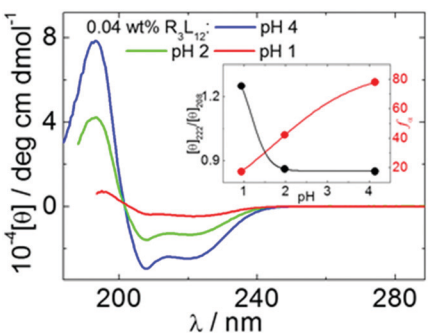

Fig. 1 CD spectra measured for 0.04 wt% R_3L_{12} at pH 4 (native), 2 and 1. The inset shows f_α and $[\theta]_{222}/[\theta]_{208}$ calculated from the CD curves.

[a] *Department of Chemistry, University of Reading, Whiteknights, Reading RG6 6AD, UK. E-mail: I.W.Hamley@reading.ac.uk*
[b] *Nanomicroscopy Center, Aalto University, Puumiehenkuja 2, FIN-02150 Espoo, Finland*
[c] *Diamond Light Source, Harwell Science and Innovation Campus, Chilton, Didcot, Oxfordshire OX11 0DE, UK*

† Electronic supplementary information (ESI) available: Experimental procedures including materials, sample preparation, experimental data obtained from several techniques (liquid MALDI-AP MS, CD, SAXS, Cryo-TEM and TEM) and tables listing the parameters extracted from the fitting to the SAXS data and the analysis of cryo-TEM images are included. See DOI: 10.1039/d0cc04299d

shown in ESI,† Fig. S1 also confirm α-helix structure).[32] For 0.04 wt% R_3L_{12}, the α-helical content f_α (and $[\theta]_{222}/[\theta]_{208}$ ratio, a measure of coiled coil aggregation[33,34]) are, respectively, 78% (0.85), 42% (0.86) and 17% (1.25) at pH 4, 2 and 1 (inset Fig. 1; the expressions used to calculate these quantities are provided in the ESI†). Decreasing the pH reduces f_α significantly, while $[\theta]_{222}/[\theta]_{208}$ increases.

Having established the conformation of SLP R_3L_{12}, we then used the powerful combination of cryo-TEM, TEM (TEM: transmission electron microscopy) and SAXS (small-angle X-ray scattering) to probe self-assembly behavior. Fig. 2 displays representative cryo-TEM images obtained for 0.04 wt% solutions of R_3L_{12} at pH 4, 2 and 1. These images (and others shown in ESI,† Fig. S2–S4) show the presence of short nanotubes at pH 4 (Fig. 2a and d). Decreasing the pH from 4 to 2 the nanotubes become better defined, and their population and length both increase (Fig. 2b, e and Fig. S3, ESI†). Decreasing the pH even further to pH 1 leads to the formation of a continuous tubular network aggregates (Fig. 2c, f and Fig. S4, ESI†).

The shape of the nanotubes at pH 2 is very well defined, several cryo-TEM images clearly show the nanotube cross section (Fig. S3, ESI†). The continuous tubular network assemblies at pH 1 seem to mainly comprise three-fold connecting nodes, such as those highlighted in Fig. S4 (ESI†). To determine the nanotube diameter and wall thickness, histograms were created (Fig. 2g and h) based on a series of cryo-TEM images for samples at each pH value. These results will be discussed below together with the parameters extracted from the fitting of the SAXS data.

Fig. 3 shows synchrotron SAXS data for 0.04 wt% solutions of R_3L_{12}. Samples at pH 4 and pH 2 present strong oscillations arising from nanotube wall interference features in the form factor, with a period set by the nanotube diameter. This features is absent from the data for the pH 1 sample, which as shown by cryo-TEM (Fig. 2) forms a tubular network structure instead of narrow dispersity diameter nanotubes. As described in detail in the ESI,† high quality form factor fits (shown as lines in Fig. 3) of the SAXS data were performed which provide the nanotube diameter, as well as wall thickness. The SAXS fitting parameters are listed in Table S1 (ESI†). Table S2 (ESI†) compares the parameters measured from cryo-TEM images with those calculated from the fitting of the SAXS curves. The results are in good agreement and these results indicate that, from TEM, the thickness of the nanotube wall, t, is 3.4 ± 0.5 nm, 3.7 ± 0.6 nm and 3.4 ± 0.5 nm pH 4, 2 and 1 respectively. From SAXS, the wall thickness is 3.3 ± 0.1 nm, 3.0 ± 0.1 nm and 3.0 ± 0.1 nm at pH 4,

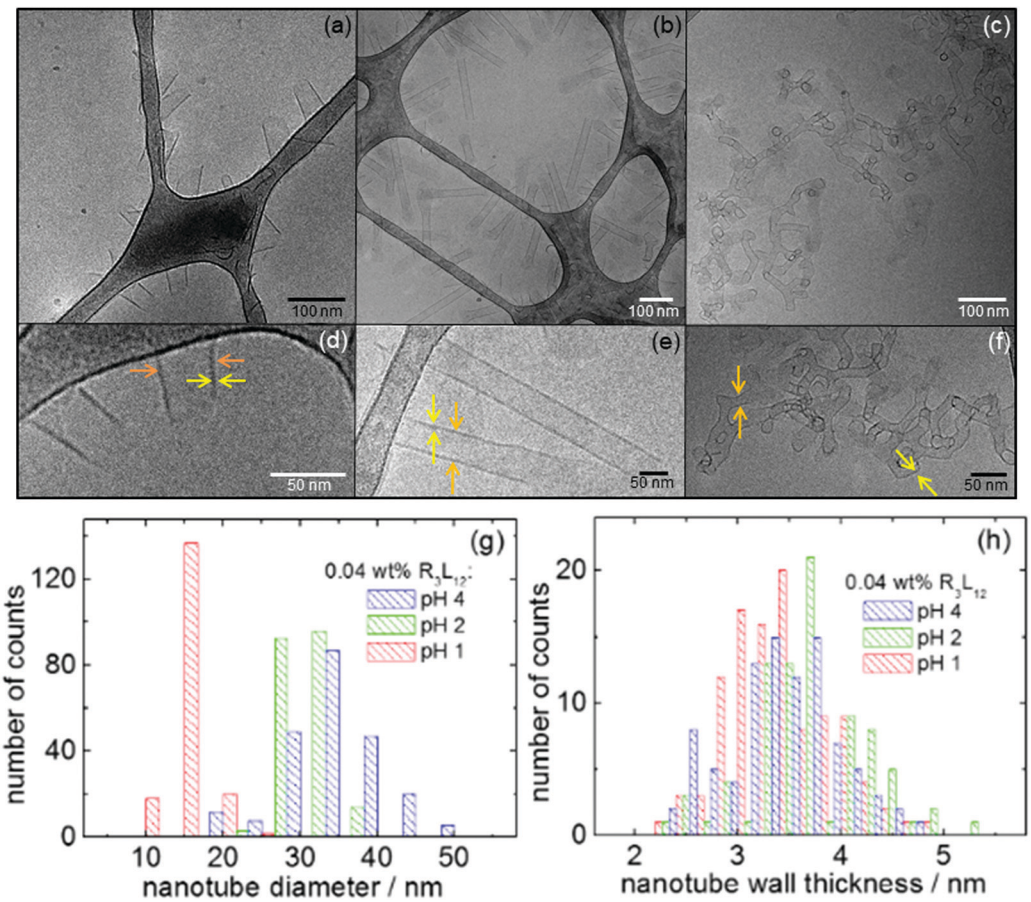

Fig. 2 Representative cryo-TEM images recorded for 0.04 wt% R_3L_{12} at pH (a and d) 4 (native), (b and e) 2 and (c and f) 1. The orange and yellow arrows indicate a nanotube diameter or the thickness of a nanotube wall respectively. Histograms showing (g) the nanotube diameter or (h) the nanotube wall thickness measured from a series of cryo-TEM images.

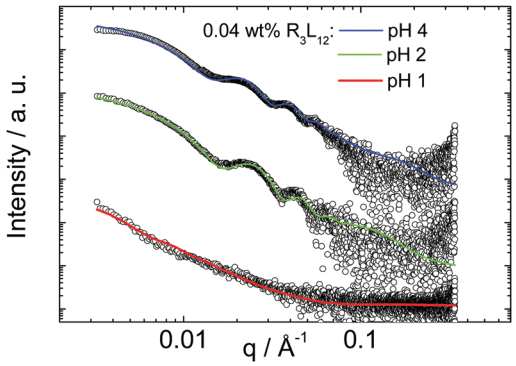

Fig. 3 SAXS spectra measured for 0.04 wt% R_3L_{12} at pH 4 (native), 2 and 1. The full lines indicate the fitting to the SAXS curves according to the models explained in the text and in the ESI.† The SAXS data has been arbitrarily shifted for clarity.

2 and 1 respectively. The diameter of the nanotube from cryo-TEM data is 32.5 ± 6.3 nm, 30.6 ± 2.8 nm and 17.4 ± 2.2 nm at pH 4, 2 and 1 respectively, and from SAXS it is 36.6 ± 3.4 nm, 33.0 ± 3.0 nm and 18.0 ± 4.0 nm respectively. These results indicate that the nanotube thickness is approximately 3 nm within the experimental error. The cryo-TEM and SAXS results also show that the nanotube diameter dramatically decreases at pH 1, *i.e.*, in the continuous tubular network structure (Fig. 2c, f and Fig. S4, ESI†). The nanotube wall thickness corresponds closely to the length of R_3L_{12} estimated using average residue spacings,[35] $l = (1.5n) + (3.4p) = 28.2$ Å (~3 nm) where $n = 12$ (number of L-residues in the α-helix) and $p = 3$ (number of R-residues).

We thus propose that the nanotube walls comprise opposed dimers of α-helices oriented perpendicular to the main axis of the nanotube, as shown in Fig. 4. The antiparallel configuration is also reasonable as it will minimize electrostatic repulsion between arginine residues (peptide charge +3 under all pH conditions studied). The nanotubes and nanotubular network structures formed are coated with arginine on inner and outer surfaces. Nanotube formation results from the balance of hydrophobic and hydrogen bonding of the leucine residues that form antiparallel coiled coil dimers and electrostatic repulsion of arginine residues. The formation of the tubular network structure at very low pH 1 is ascribed to the unfavorable electrostatic penalty associated with having uncapped tubes exposed to large H^+ ion concentrations, leading to closure into tubular networks.

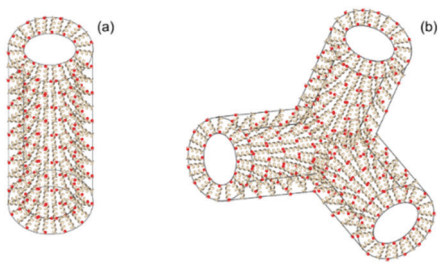

Fig. 4 (a) Model for nanotube formed with a wall of antiparallel α-helical peptide dimers radially oriented perpendicular to the main axis of the nanotube (0.04 wt% R_3L_{12} at pH 2 and 4). (b) Model for three-fold node in the tubular network structure (0.04 wt% R_3L_{12} at pH 1).

Remarkably, distinct structures were observed in dried films of the pH 1 sample. TEM images (representative examples shown in Fig. S5, ESI†) consistently showed a population of sheet structures containing prominent lattices with square arrays 3 nm × 3 nm in size. This size corresponds approximately to the estimated length of an antiparallel α-helical dimer,[35] considering the closely packed leucine residues, but allowing for splaying of the longer terminal arginine residues. We propose that this structure is a rotator-type phase, in which electrostatic repulsion of arginine residues is minimized by 90° rotations of helical dimers (Fig. S5c, ESI†), analogous, for example, to certain 2D spin lattice nanomagnet systems.[36] We propose that this structure is favored in dried films due to confinement which leads to α-helices parallel to the interface, whereas in bulk the helical dimers are able to orient perpendicular to the nanotube surfaces.

Additional studies were performed on solutions containing a higher concentration, 0.07 wt%, of R_3L_{12}. Fig. S6–S8 (ESI†) display cryo-TEM and fitted SAXS form factor data. Nanotube parameters obtained from the fitting to the SAXS curves and measures of the cryo-TEM images are listed in Tables S1 and S2 (ESI†). Cryo-TEM images at pH 4 show unwrapped nanotubes (Fig. S6, ESI†), coexisting with a population of short folded nanotubes (inset Fig. S6a, ESI†). Increasing the pH to 2 gives well defined long nanotubes (Fig. S7a–c, ESI†), and a tubular structure network is formed at pH 1 (Fig. S8, ESI†). These results are similar to those at the lower concentration 0.04 wt%, with the exception of the unwrapped nanotubes observed at pH 4. This points to the subtle interplay of electrostatic and hydrophobic interactions, modulated by peptide concentration. Nanotube dimensions were obtained from cryo-TEM and SAXS (Fig. S7d, e, S8c, d and Tables S1 and S2, ESI†) and are generally very similar to those measured for 0.04 wt% R_3L_{12} samples, as discussed above. Analysis of CD spectra (Fig. 1 and ESI,† Fig. S1) indicates that there is a slight increase in α-helical content and a stronger tendency to form coiled coil helices at 0.07 wt% compared to 0.04 wt% peptide. The stability of R_3L_{12} in very acidic solution (pH 1) was investigated using state-of-the-art liquid AP-MALDI MS. The spectra shown in ESI,† Fig. S9 show that no peptide degradation was detectable for the solutions at pH 4 or 1.

In summary, designed SLP R_3L_{12} exhibits remarkable pH-dependent self-assembly of α-helical peptide structures, including nanotubes and tubular network structures with molecular thickness arginine-coated walls based on opposed dimeric coiled coils. Our results contrast with observations for the related peptide K_3L_{12} which forms bilayer discs, fibrils or vesicles depending on pH, resulting from self-assembly of α-helical peptides.[37] It is also distinct from the behavior of longer "block" polypeptides such as $R_{60}L_{20}$ which self-assembles to form vesicles.[38] The self-assembly of SLP R_3L_{12} can also be contrasted with conventional coiled coil peptides with heptad repeats which can be engineered to form extended coiled–coil assemblies, such as fibrils and nanotubes,[24,39–42] since these generally contain arrays of helices

parallel to the long axis, although radial arrangements have been reported,[43] in particular in the recently discovered cross-α fibril structure.[44] Peptide R_3L_{12} forms distinctive cross-α nanotube structures. As well as remarkable self-assembly properties, R_3L_{12} may have interesting bioactivities and functionalities (for example potential cell-penetrating, antimicrobial or biocatalytic activities) arising from the high-density arginine-coating of the nanotubes and tube networks.

The work of VC was supported by EPSRC Platform grant EP/L020599/1 ''Nanostructured Polymeric Materials for Healthcare'' to IWH. We are grateful Diamond for beamtime on B21 (ref. SM22925-1). We acknowledge access to the Chemical Analysis Facility Laboratory (Univ. of Reading).

Conflicts of interest

There are no conflicts to declare.

Notes and references

1 M. R. Ghadiri, J. R. Granja and L. K. Buehler, *Nature*, 1994, **369**, 301–304.
2 D. T. Bong, T. D. Clark, J. R. Granja and M. R. Ghadiri, *Angew. Chem., Int. Ed.*, 2001, **40**, 988–1011.
3 M. Reches and E. Gazit, *Science*, 2003, **300**, 625–627.
4 X. Gao and H. Matsui, *Adv. Mater.*, 2005, **17**, 2037–2050.
5 T. Shimizu, M. Masuda and H. Minamikawa, *Chem. Rev.*, 2005, **105**, 1401–1443.
6 S. Scanlon and A. Aggeli, *Nano Today*, 2008, **3**, 22–30.
7 R. J. Brea, C. Reiriz and J. R. Granja, *Chem. Soc. Rev.*, 2010, **39**, 1448–1456.
8 X. H. Yan, P. L. Zhu and J. B. Li, *Chem. Soc. Rev.*, 2010, **39**, 1877–1890.
9 G. Rosenman, P. Beker, I. Koren, M. Yevnin, B. Bank-Srour, E. Mishina and S. Semin, *J. Pept. Sci.*, 2011, **17**, 75–87.
10 C. Valéry, F. Artzner and M. Paternostre, *Soft Matter*, 2011, **7**, 9583–9594.
11 K. L. Morris, S. Zibaee, L. Chen, M. Goedert, P. Sikorski and L. C. Serpell, *Angew. Chem., Int. Ed.*, 2013, **52**, 2279–2283.
12 I. W. Hamley, *Angew. Chem., Int. Ed.*, 2014, **53**, 6866–6881.
13 L. Adler-Abramovich and E. Gazit, *Chem. Soc. Rev.*, 2014, **43**, 6881–6893.
14 P. Zelenovskiy, I. Kornev, S. Vasilev and A. Kholkin, *Phys. Chem. Chem. Phys.*, 2016, **18**, 29681–29685.
15 K. Lu, J. Jacob, P. Thiyagarajan, V. P. Conticello and D. G. Lynn, *J. Am. Chem. Soc.*, 2003, **125**, 6391–6393.
16 M. J. Krysmann, V. Castelletto, J. M. E. McKendrick, I. W. Hamley, C. Stain, P. J. F. Harris and S. M. King, *Langmuir*, 2008, **24**, 8158–8162.
17 A. K. Mehta, K. Lu, W. S. Childers, S. Liang, J. Dong, J. P. Snyder, S. V. Pingali, P. Thiyagarajan and D. G. Lynn, *J. Am. Chem. Soc.*, 2008, **130**, 9829–9835.
18 I. W. Hamley, A. Dehsorkhi, V. Castelletto, S. Furzeland, D. Atkins, J. Seitsonen and J. Ruokolainen, *Soft Matter*, 2013, **9**, 9290–9293.
19 I. W. Hamley, A. Dehsorkhi and V. Castelletto, *Chem. Commun.*, 2013, **49**, 1850–1852.
20 J. Madine, V. Castelletto, I. W. Hamley and D. A. Middleton, *Angew. Chem., Int. Ed.*, 2013, **52**, 10537–10540.
21 C. Valery, M. Paternostre, B. Robert, T. Gulik-Krzywicki, T. Narayanan, J. C. Dedieu, G. Keller, M. L. Torres, R. Cherif-Cheikh, P. Calvo and F. Artzner, *Proc. Natl. Acad. Sci. U. S. A.*, 2003, **100**, 10258–10262.
22 C. Tarabout, S. Roux, F. Gobeaux, N. Fay, E. Pouget, C. Meriadec, M. Ligeti, D. Thomas, M. Ijsselstijn, F. Besselievre, D. A. Buisson, J. M. Verbavatz, M. Petitjean, C. Valery, L. Perrin, B. Rousseau, F. Artzner, M. Paternostre and J. C. Cintrat, *Proc. Natl. Acad. Sci. U. S. A.*, 2011, **108**, 7679–7684.
23 J. D. Hartgerink, J. R. Granja, R. A. Milligan and M. R. Ghadiri, *J. Am. Chem. Soc.*, 1996, **118**, 43–50.
24 C. F. Xu, R. Liu, A. K. Mehta, R. C. Guerrero-Ferreira, E. R. Wright, S. Dunin-Horkawicz, K. Morris, L. C. Serpell, X. B. Zuo, J. S. Wall and V. P. Conticello, *J. Am. Chem. Soc.*, 2013, **135**, 15565–15578.
25 N. C. Burgess, T. H. Sharp, F. Thomas, C. W. Wood, A. R. Thomson, N. R. Zaccai, R. L. Brady, L. C. Serpell and D. N. Woolfson, *J. Am. Chem. Soc.*, 2015, **137**, 10554–10562.
26 M. Nambiar, M. Nepal and J. Chmielewski, *ACS Biomater. Sci. Eng.*, 2019, **5**, 5082–5087.
27 S. Santoso, W. Hwang, H. Hartman and S. Zhang, *Nano Lett.*, 2002, **2**, 687–691.
28 V. Castelletto, R. H. Barnes, K. A. Karatzas, C. J. C. Edwards-Gayle, F. Greco, I. W. Hamley, R. Rambo, J. Seitsonen and J. Ruokolainen, *Biomacromolecules*, 2018, **19**, 2782–7294.
29 V. Castelletto, C. J. C. Edwards-Gayle, I. W. Hamley, G. Barrett, J. Seitsonen and J. Ruokolainen, *ACS Appl. Mater. Interfaces*, 2019, **11**, 9893–9903.
30 J. Madine, H. A. Davies, C. Shaw, I. W. Hamley and D. A. Middleton, *Chem. Commun.*, 2012, **48**, 2976–2978.
31 P. Y. Chou and G. D. Fasman, *Biochemistry*, 1974, **13**, 222–245.
32 S. M. Kelly, T. J. Jess and N. C. Price, *Biochim. Biophys. Acta*, 2005, **1751**, 119–139.
33 J. Y. Su, R. S. Hodges and C. M. Kay, *Biochemistry*, 1994, **33**, 15501–15510.
34 G. Vandermeulen, C. Tziatzios and H. Klok, *Macromolecules*, 2003, **36**, 4107–4114.
35 T. E. Creighton, *Proteins. Structures and Molecular Properties*, W. H. Freeman, New York, 1993.
36 J. M. Porro, S. A. Morley, D. A. Venero, R. Macedo, M. C. Rosamond, E. H. Linfield, R. L. Stamps, C. H. Marrows and S. Langridge, *Sci. Rep.*, 2019, **9**, 11.
37 H. C. Fry, G. d. Q. Silveira, H. M. Cohn and B. Lee, *Langmuir*, 2019, **35**, 8961–8967.
38 E. P. Holowka, V. Z. Sun, D. T. Kamei and T. J. Deming, *Nat. Mater.*, 2007, **6**, 52–57.
39 M. J. Pandya, G. M. Spooner, M. Sunde, J. R. Thorpe, A. Rodger and D. N. Woolfson, *Biochemistry*, 2000, **39**, 8728–8734.
40 D. N. Woolfson, *Adv. Protein Chem.*, 2005, **70**, 79–112.
41 Y. Y. Wu, P. K. Norberg, E. A. Reap, K. L. Congdon, C. N. Fries, S. H. Kelly, J. H. Sampson, V. P. Conticello and J. H. Collier, *ACS Biomater. Sci. Eng.*, 2017, **3**, 3128–3132.
42 Y. Tian, F. B. Polzer, H. V. Zhang, K. L. Kiick, J. G. Saven and D. J. Pochan, *Biomacromolecules*, 2018, **19**, 4286–4298.
43 E. H. Egelman, C. Xu, F. DiMaio, E. Magnotti, C. Modlin, X. Yu, E. Wright, D. Baker and V. P. Conticello, *Structure*, 2015, **23**, 280–289.
44 E. Tayeb-Fligelman, O. Tabachnikov, A. Moshe, O. Goldshmidt-Tran, M. R. Sawaya, N. Coquelle, J. P. Colletier and M. Landau, *Science*, 2017, **355**, 831–833.

